Uncovering the Kuramoto Model from Full-order Models of Grid-forming Inverter-based Power Networks

Olaoluwapo Ajala Nathan Baeckeland Sairaj Dhople Alejandro Domínguez-García

***Abstract*— This paper presents parametric assumptions under which the classical Kuramoto model can be uncovered from full-order models of an interconnected group of grid-forming inverters based on droop control, virtual synchronous machine control and/or dispatchable virtual oscillator control. The equivalence is established with reduced-order models that are derived by leveraging singular-perturbation analysis, time-domain Kron reduction of the network dynamics, and a particular control configuration that is based on the inductance-to-resistance ratio of interconnecting transmission lines. Numerical results compare the phase and frequency response of the full-order model and the reduced-order Kuramoto model.**

I. Introduction

The emergence of inverter-based generating resources in power systems has led to a transformation of the electric power grid. In particular, transitions from synchronous power generators to grid-forming (GFM) inverter-interfaced counterparts, whose underlying control systems are significantly different, have altered the dynamic characteristics of the electric power grid. Characterizing and projecting the impact of changes brought about by integration of GFM inverters can be greatly facilitated by identifying equivalences, if they exist, between dynamic behavior of the GFM inverters and that of prototypical and classical dynamical systems which have well-studied attributes.

One such classical system is a network of nonlinear coupled oscillators whose dynamics are described by the so-called *Kuramoto Model* [1]. We provide a brief description of such a model. Consider a group of n coupled oscillators, and let ω_0 denote their nominal frequency. Also, let ω_i denote the natural frequency of oscillator i. Let $a_{ij} \geq 0$ denote the coupling strength between oscillators i and j, with $a_{ij} = a_{ji}$, and let δ_i denote the phase of oscillator i, relative to a reference frame rotating at frequency ω_0. Then, the Kuramoto Model is described by the relation:

$$\dot{\delta}_i = \omega_i - \omega_0 - \sum_{j=1}^{n} a_{ij} \sin(\delta_i - \delta_j), \quad i \in \{1, 2, \ldots, n\}. \quad (1)$$

O Ajala and A. Domínguez-García are with the Department of Electrical and Computer Engineering, University of Illinois at Urbana-Champaign, Urbana, IL 61801 USA. E-mail:{ooajala2, aledan}@ILLINOIS.EDU.

N. Baeckeland is with the Department of Electrical Engineering, Katholieke Universiteit Leuven (KU Leuven), 3000 Leuven, Belgium. Email: nathan.baeckeland@KULEUVEN.BE.

S. Dhople is with the Department of Electrical and Computer Engineering, University of Minnesota, Minneapolis, MN 55455 USA. Email: sdhople@UMN.EDU.

This work was supported in part by the U.S. Department of Energy's Office of Energy Efficiency and Renewable Energy (EERE) under Solar Energy Technologies Office (SETO) Agreement Number EE0009025.

The main contribution of this paper is to demonstrate how a Kuramoto model can be recovered from the full-order model of an interconnected and diverse group of GFM inverter-based resources. We show that there exists an equivalence between the dynamics of such power networks and those of the Kuramoto model. Electrical networks based on three well-known GFM inverter technologies, droop control [2], virtual synchronous machine (VSM) control [3], and dispatchable virtual oscillator control (dVOC) [4], are considered. Full-order models are developed for a group of such GFM inverters that are interconnected via transmission lines with a homogeneous inductance-to-resistance ratio, and singular perturbation analysis as well as time-domain Kron-reduction are employed to derive the Kuramoto model While there is a vast body of work in the literature that establishes an equivalence between the dynamics of the power grid and those of the Kuramoto model, to the best of our knowledge, these do not consider a diverse mix of GFM inverter-based resources, present the relevant assumptions, and rigorously demonstrate the model-order reduction steps that are involved in recovering the Kuramoto model from the originating full-order models.

Prior efforts have investigated equivalence of different GFM control types [5], [6]. The focus of this paper, however, is to establish an equivalence between GFM control models and the Kuramoto model presented in (1). This has been attempted in varying degrees for a wide class of power grid models in the literature. In [7], the dynamics of the so-called gradient system, which is used in transient stability analysis of a power system, and whose corresponding set of equations are equivalent to those of the Kuramoto model, are presented. However, the underlying electrical network is based on synchronous generators, and the authors do not point out its equivalence with the Kuramoto model—decades later, authors in [8] identify the connection. In [9], [10], authors show that the dynamics of droop-controlled inverters are equivalent to those of the Kuramoto model. However, in [9], [10] only inverters based on droop control are considered, and in [9], the Kuramoto-type model is not derived from the full-order model, and the inverters are assumed to be connected in a star topology. Compared to the prior art surveyed above, we demonstrate how to rigorously derive the Kuramoto model from full-order models of GFM inverter-based power networks.

II. Preliminaries

In this section, we describe the notation and reference-frame transformations that are used in this paper.

A. Notation

Consider a vector $x \in \mathbb{R}^n$, whose elements are $x_1, \ldots, x_n$; then we define $\mathbf{sin}(x) = [\sin(x_1), \ldots, \sin(x_n)]^\top$, $\mathbf{cos}(x) = [\cos(x_1), \ldots, \cos(x_n)]^\top$, $\mathbf{arcsin}(x) = [\arcsin(x_1), \ldots, \arcsin(x_n)]^\top$, $\mathbf{T}(x) = [\mathbf{cos}(x), \mathbf{sin}(x)]^\top$. We let $\mathrm{diag}(x)$ denote the $n \times n$ diagonal matrix whose diagonal elements comprise elements of $x \in \mathbb{R}^n$. The identity matrix is denoted by $\mathbb{I}$, the standard basis vector with one in the i-th position is denoted by $\mathbb{e}_i$, and the all-zeros and all-ones vectors are denoted by $\mathbb{O}$ and $\mathbb{1}$, respectively. (Dimensions of these constructs are left unspecified since they can be inferred from the context.) *The dynamical models presented in the remainder of this paper have been normalized, with all parameters and variables presented in a per-unit transcription (see, e.g., [11, p. 75]).*

B. Reference-frame transformations

Consider the three-phase signal $f_{abc} = [f_a\,, f_b\,, f_c]^\top$, where f_a, f_b, and f_c form a balanced three-phase set. Let ω_0 and ω denote the nominal angular frequency and the GFM inverter's angular frequency, both measured in $\mathrm{rad\,s^{-1}}$, respectively. We let

$$f_{DQ} = [f_D\,, f_Q]^\top \quad \text{and} \quad f_{dq} := [f_d\,, f_q]^\top$$

denote the dq transformations of f_{abc} to reference frames rotating at angular frequencies ω_0 and ω, respectively (see [12], pp. 69–114 for more details). Define

$$\delta = \int_0^t (\omega(\tau) - \omega_0)\, d\tau + \delta_0, \tag{2}$$

where δ_0 denotes the initial condition of δ; then, signals in the DQ and dq reference frames are related to the three-phase signal via

$$f_{dq} = \mathrm{T}(\delta) f_{DQ}, \quad f_{dq} = \overline{\mathrm{T}}(\delta + \omega_0 t) f_{abc}, \tag{3}$$

where rotation matrices $\mathrm{T}(\cdot)$ and $\overline{\mathrm{T}}(\cdot)$ are defined as

$$\mathrm{T}(\theta) = \begin{bmatrix} \cos\theta & \sin\theta \\ -\sin\theta & \cos\theta \end{bmatrix},$$

$$\overline{\mathrm{T}}(\theta) = \frac{2}{3}\begin{bmatrix} \cos\theta & \cos(\theta - \frac{2\pi}{3}) & \cos(\theta + \frac{2\pi}{3}) \\ -\sin\theta & -\sin(\theta - \frac{2\pi}{3}) & -\sin(\theta + \frac{2\pi}{3}) \end{bmatrix}.$$

III. The Electrical Network Model

In this section, we present the model for the electrical network interconnecting the GFM inverters.

A. Graph-theoretic network model

Consider an electric power network comprising b buses ($b > 1$) that are interconnected via l transmission lines. Without loss of generality, assume there is at most one transmission line connecting each pair of buses. Assign an arbitrary direction for the positive flow of power along each transmission line. Then, the topology of the electrical network together with the chosen orientation can be described by a connected directed graph $\mathcal{G} = (\mathcal{V}, \mathcal{E})$, with $\mathcal{V} = \{1, 2, \ldots, b\}$ denoting the set of buses, and $\mathcal{E} \subset \mathcal{V} \times \mathcal{V} \setminus \{(i,i) : i \in \mathcal{V}\}$ denoting the set of transmission lines so that $(i,j) \in \mathcal{E}$ if buses i and j are electrically connected, with the flow of power from bus i to bus j assigned to be positive. Let $\mathbb{L}$ denote a one-to-one mapping from $\mathcal{E}$ to $\mathcal{L} = \{1, 2, \ldots, l\}$ so that, for each $(i,j) \in \mathcal{E}$, there exists a unique $k \in \mathcal{L}$ that satisfies $k = \mathbb{L}(i,j)$. Accordingly, we can define a node-to-edge incidence matrix, denoted by $M = [m_{ik}] \in \mathbb{R}^{b \times l}$, as follows:

$$\begin{aligned} m_{ik} &= 1, && \text{if } k = \mathbb{L}(i,j), \quad (i,j) \in \mathcal{E}, \\ m_{ik} &= -1, && \text{if } k = \mathbb{L}(j,i), \quad (j,i) \in \mathcal{E}, \\ m_{ik} &= 0, && \text{otherwise.} \end{aligned}$$

B. Dynamical model

We consider the case when all transmission lines in the electrical network are short and have homogeneous inductance-to-resistance ratios.[1] As a result, each line $i \in \mathcal{L}$ can be described using a series resistance and inductance, denoted by r_i and l_i, respectively, that satisfies the relation

$$\frac{l_i}{r_i} = \frac{l_j}{r_j}, \quad \forall i, j \in \mathcal{L}.$$

We will find it useful to define the time constant associated with the transmission lines, which we denote as τ_ℓ, and the angle associated with the transmission line impedance at frequency ω_0, which we denote as φ, as follows:

$$\tau_\ell = \frac{l_i}{\omega_0 r_i}, \quad \forall i \in \mathcal{L}; \qquad \varphi = \arctan\left(\tau_\ell \omega_0\right). \tag{4}$$

Let $v_{DQ,i}$ and $i_{DQ,i}$ denote the dq transformations of the voltage and current injection at bus i of the electrical network, respectively; with these, we define the matrices

$$\begin{aligned} V_{DQ} &= \begin{bmatrix} v_{DQ,1}, & v_{DQ,2}, & \ldots, & v_{DQ,b} \end{bmatrix} \in \mathbb{R}^{2 \times b}, \\ I_{DQ} &= \begin{bmatrix} i_{DQ,1}, & i_{DQ,2}, & \ldots, & i_{DQ,b} \end{bmatrix} \in \mathbb{R}^{2 \times b}, \\ R &= \mathrm{diag}\big(r_1, \; r_2, \; \ldots, \; r_l\big) \in \mathbb{R}^{l \times l}, \\ L &= \mathrm{diag}\big(l_1, \; l_2, \; \ldots, \; l_l\big) \in \mathbb{R}^{l \times l}. \end{aligned}$$

Applying Kirchhoff's laws to each bus in the electrical network yields the following dynamical model for transmission lines in the network:

$$\tau_\ell \dot{I}_{DQ} = \big(\tau_\ell \omega_0 \mathrm{T}(\tfrac{\pi}{2}) - \mathbb{I}\big) I_{DQ} + V_{DQ} M R^{-1} M^\top. \tag{5}$$

IV. The Grid-forming Inverter Model

In this section, we present full-order dynamical models for GFM inverters that cover the dynamics of droop, VSM, and dVOC strategies, and also includes detailed models of all other control- and physical-layer subsystems.[2] The full-order models are based on developments in [2]–[4], [12].

[1] A transmission line is typically categorized as *short* if its effective length is less than 50 miles (80 km) [11, p. 208].

[2] Given that the electrical network includes multiple GFM inverters, all variables and parameters associated with the GFM inverter model ought to be indexed accordingly. However, we exclude such indexing from the models presented in this section to contain notational burden.

A. Overview

The architecture of the GFM inverter examined in this work is depicted in Fig. 1. The GFM inverter is voltage sourced and includes a control system, which sends signals via a pulse width modulation (PWM) module to the switches (not depicted), and an LCL filter, which limits high-order harmonics in the output. The control system comprises: i) a primary controller, with dynamics that may be based on droop (the blue-colored box), VSM (the red-colored box), or dVOC (the green-colored box); ii) two internal proportional-integral (PI) controllers to regulate voltage and current; and iii) dq-to-abc transformations based on (3).

B. Primary controller dynamics

Let p and q denote the active- and reactive-power delivered to the grid at the filter's capacitor terminals, and let p_{m} and q_{m} denote their measured values, respectively. We define $s = [p,\, q]^\top$ and $s_{\mathrm{m}} = [p_{\mathrm{m}},\, q_{\mathrm{m}}]^\top$. References for active power, and reactive power are denoted by $p^\star$ and $q^\star$, respectively, and we define $s^\star = [p^\star, q^\star]^\top$. The voltage-magnitude reference is denoted by $e^\star$. Also, let e_0 and ω_0 denote the nominal inverter voltage magnitude and the nominal frequency, in per-unit and $\mathrm{rad\,s^{-1}}$, respectively. In addition, let $\psi \in [0, 2\pi)$ denote a rotation angle that, in steady state and when $\psi = \frac{\pi}{2}$, imposes a correlation between active power and frequency, and between reactive power and voltage ($\psi = 0$ does the polar opposite) [4]. While there is flexibility in the choice of ψ based on desired terminal behavior, we will find in subsequent developments that setting it equal to φ (see (4)) is a key step to recovering the Kuramoto model. Next, we describe the dynamics of the three primary control strategies.

1) Droop Control: The droop dynamics are described by:

$$\omega = \omega_0 + \frac{1}{d_{\mathrm{f}}} \mathbb{e}_1^\top \mathrm{T}(\psi - \tfrac{\pi}{2})(s^\star - s_{\mathrm{m}}), \tag{6a}$$

$$e^\star = e_0 + \frac{1}{d_{\mathrm{v}}} \mathbb{e}_2^\top \mathrm{T}(\psi - \tfrac{\pi}{2})(s^\star - s_{\mathrm{m}}), \tag{6b}$$

$$\frac{1}{\omega_{\mathrm{c}}} \dot{s}_{\mathrm{m}} = -s_{\mathrm{m}} + s, \tag{6c}$$

where ω_{c} denotes the cut-off frequency of a low-pass measurement filter, in units of $\mathrm{rad\,s^{-1}}$, and d_{f}, d_{v} denote droop coefficients for frequency and voltage, in units of $\mathrm{s\,rad^{-1}}$ and $\mathrm{V^{-1}}$, respectively.

2) Virtual Synchronous Machine (VSM) Control: VSM control typically involves a phase-locked loop (PLL) to compute the frequency of the grid. Let $v_{\mathrm{g}dq}$ denote the grid-side voltage, η denote the internal state variable of the PLL, and α denote the output phase of the PLL. Then, VSM control dynamics are described by:

$$\begin{aligned}\frac{m_{\mathrm{f}}}{d_{\mathrm{f}}} \dot{\omega} =& -\omega + \omega_0 + \frac{d_{\mathrm{d}}}{d_{\mathrm{f}}} \left(k_{\mathrm{P}} \dot{\eta} + \omega_0 k_{\mathrm{I}} \eta\right) \\ &+ \frac{1}{d_{\mathrm{f}}} (\mathbb{e}_1^\top \mathrm{T}(\psi - \tfrac{\pi}{2})(s^\star - s)),\end{aligned} \tag{7a}$$

$$e^\star = e_0 + \frac{1}{d_{\mathrm{v}}} \mathbb{e}_2^\top \mathrm{T}(\psi - \tfrac{\pi}{2})(s^\star - s_{\mathrm{m}}), \tag{7b}$$

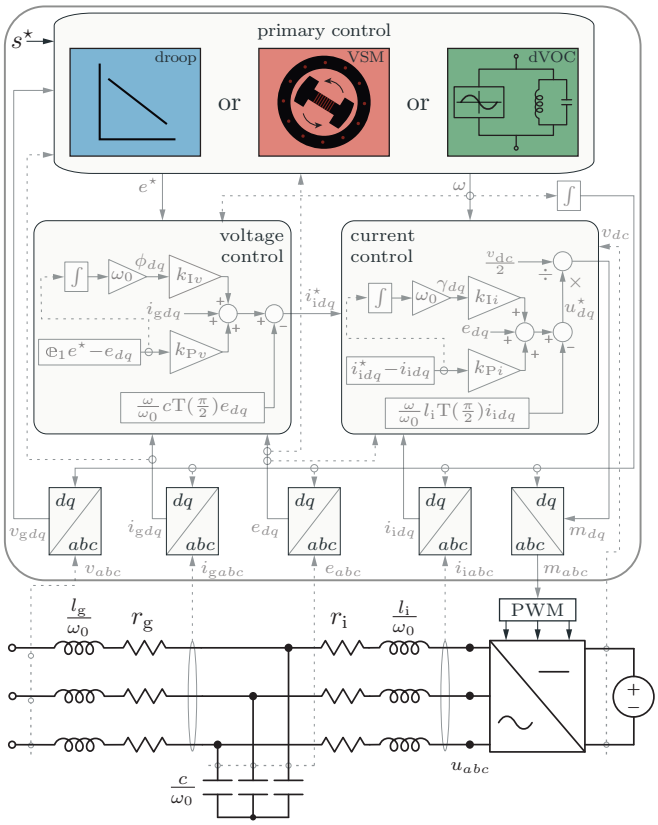

Fig. 1: A schematic diagram of the full-order GFM-inverter model. The voltages across the DC and AC side of the inverter are denoted by v_{dc} and u_{abc}. The PWM module input signal is denoted by m_{abc}. State variables for the PI controllers are denoted as ϕ_{dq} and γ_{dq}, respectively; corresponding PI gains are denoted by $k_{\mathrm{P}v}, k_{\mathrm{I}v}$ and $k_{\mathrm{P}i}, k_{\mathrm{I}i}$, respectively. The voltage reference for the three-phase inverter is denoted by $u^\star_{dq}$. The inverter- and grid-side currents are denoted by $i_{\mathrm{i}abc}$ and $i_{\mathrm{g}abc}$, respectively; voltage of the filter-capacitor, c, is denoted e_{abc}, and the bus voltage is denoted v_{abc}. The inverter-side resistance and inverter-side inductance are denoted as r_{i}, and l_{i}, respectively. The sum of resistive and inductive elements (from the filter and transmission line) on the grid side are denoted by r_{g} and l_{g}, respectively.

$$\frac{1}{\omega_{\mathrm{c}}} \mathbb{e}_2^\top \dot{s}_{\mathrm{m}} = -\mathbb{e}_2^\top s_{\mathrm{m}} + \mathbb{e}_2^\top s, \tag{7c}$$

$$\frac{1}{\omega_0} \dot{\eta} = \mathbb{e}_2^\top \mathrm{T}(\alpha) v_{\mathrm{g}dq}, \tag{7d}$$

$$\frac{1}{\omega_0} \dot{\alpha} = \frac{k_{\mathrm{P}}}{\omega_0} \dot{\eta} + k_{\mathrm{I}} \eta, \tag{7e}$$

where d_{d} denotes the damping coefficient, in units of $\mathrm{s\,rad^{-1}}$, k_{P} and k_{I} denote the proportional and integral gains of the PLL, in per-unit, respectively, m_{f} denotes the mechanical time constant, in units of $\mathrm{s^2\,rad^{-1}}$. Note that ω_{c}, d_{f}, and d_{v} have the same interpretation as in droop control.

3) Dispatchable Virtual Oscillator Control: The dVOC dynamics are described by:

$$\omega = \omega_0 + \frac{\omega_0 \kappa_1}{(e^\star)^2} \mathbb{e}_1^\top \mathrm{T}(\psi - \tfrac{\pi}{2})(s^\star - s), \tag{8a}$$

$$\frac{1}{\omega_0} \dot{e}^\star = \frac{\kappa_1}{e^\star} \mathbb{e}_2^\top \mathrm{T}(\psi - \tfrac{\pi}{2})(s^\star - s) + \kappa_2 e^\star (e_0^2 - (e^\star)^2), \tag{8b}$$

where κ_1 and κ_2 denote the synchronization gain and the voltage-amplitude control gain, in per-unit, respectively.

TABLE I: Universal primary control model and parametric assumptions under which it boils down to droop, VSM, and dVOC.

$$
\begin{aligned}
\boldsymbol{\tau_{\mathrm{f}}}\dot{\omega} &= -\omega+\omega_0+\boldsymbol{\kappa_{\mathrm{d}}}\big(k_{\mathrm{P}}\dot{\eta}+\omega_0 k_{\mathrm{I}}\eta\big)\\
&\quad+\boldsymbol{\kappa_{\mathrm{f}}}\mathbb{e}_1^\top \mathrm{T}(\psi-\tfrac{\pi}{2})(s^\star-s_{\mathrm{m}}),\\
\boldsymbol{\tau_{\mathrm{v}}}\dot{e}^\star &= \boldsymbol{\kappa_{\mathrm{v}}}\mathbb{e}_2^\top \mathrm{T}(\psi-\tfrac{\pi}{2})(s^\star-s_{\mathrm{m}})\\
&\quad+\boldsymbol{f_{\mathrm{v}}}(\boldsymbol{e^\star}),\\
\boldsymbol{\tau_{\mathrm{p}}}\dot{s}_{\mathrm{m}} &= -s_{\mathrm{m}}+s,\\
\frac{1}{\omega_0}\dot{\eta} &= \mathbb{e}_2^\top \mathrm{T}(\alpha)v_{\mathrm{g}dq},\\
\frac{1}{\omega_0}\dot{\alpha} &= \frac{k_{\mathrm{P}}}{\omega_0}\dot{\eta}+k_{\mathrm{I}}\eta.
\end{aligned}
\tag{9}
$$

universal primary control

	$\boldsymbol{\tau_{\mathrm{f}}}$	$\boldsymbol{\tau_{\mathrm{v}}}$	$\boldsymbol{\tau_{\mathrm{p}}}$	$\boldsymbol{\kappa_{\mathrm{d}}}$	$\boldsymbol{\kappa_{\mathrm{f}}}$	$\boldsymbol{\kappa_{\mathrm{v}}}$	$\boldsymbol{f_{\mathrm{v}}(e^\star)}$
droop	0	0	$\frac{1}{\omega_{\mathrm{c}}}$	0	$\frac{1}{d_{\mathrm{f}}}$	$\frac{1}{d_{\mathrm{v}}}$	$-e^\star+e_0$
VSM	$\frac{m_{\mathrm{f}}}{d_{\mathrm{f}}}$	0	$\frac{1}{\omega_{\mathrm{c}}}$	$\frac{d_{\mathrm{d}}}{d_{\mathrm{f}}}$	$\frac{1}{d_{\mathrm{f}}}$	$\frac{1}{d_{\mathrm{v}}}$	$-e^\star+e_0$
dVOC	0	$\frac{1}{\omega_0}$	0	0	$\frac{\omega_0\kappa_1}{(e^\star)^2}$	$\frac{\kappa_1}{e^\star}$	$\kappa_2(-(e^\star)^2+e_0^2)e^\star$

Universal Primary Control Model. We can define a model whose dynamics, under certain parametric assumptions, boil down to those of droop, VSM, or dVOC discussed above. We refer to such a model as the *universal primary control model*. Let τ_{f}, τ_{v}, and τ_{p} denote time constants for the frequency, voltage, and power control dynamics, respectively, in units of $\mathrm{s\,rad^{-1}}$. Let κ_{d} denote the ratio of the damping and frequency droop coefficients, in per-unit; let κ_{f} and κ_{v} represent the (inverse) frequency and voltage droop coefficients of the primary control, in $\mathrm{rad\,s^{-1}}$ and per-unit, respectively; and let $f_{\mathrm{v}}(\cdot)$ denote a function whose output represents a measure of the deviation of its argument from e_0. Then, the dynamics of the universal primary control model are described by (10) in Table I, with the parametric assumptions under which droop, VSM, and dVOC are recovered listed alongside.

C. Filter, voltage- and current-controller dynamics

The averaged dynamics of the LCL filter, voltage controller, and the current controller depicted in Fig. 1 are described compactly by

$$\frac{l_{\mathrm{i}}}{\omega_0 r_{\mathrm{i}}}\dot{i}_{\mathrm{i}dq} = -i_{\mathrm{i}dq}+\frac{k_{\mathrm{P}i}}{\omega_0 r_{\mathrm{i}}}\dot{\gamma}_{dq}+\frac{k_{\mathrm{I}i}}{r_{\mathrm{i}}}\gamma_{dq}, \tag{10a}$$

$$\frac{c}{\omega_0}\dot{e}_{dq} = \frac{\omega c}{\omega_0}\mathrm{T}(\tfrac{\pi}{2})e_{dq}+(i_{\mathrm{i}dq}-i_{\mathrm{g}dq}), \tag{10b}$$

$$\frac{1}{\omega_0 k_{\mathrm{I}v}}\dot{\phi}_{dq} = \frac{1}{k_{\mathrm{I}v}}\mathbb{e}_1 e^\star-\frac{1}{k_{\mathrm{I}v}}c\mathrm{T}(\tfrac{\pi}{2})e_{dq}, \tag{10c}$$

$$\begin{aligned}\frac{1}{\omega_0 k_{\mathrm{I}v}}\dot{\gamma}_{dq} &= \frac{k_{\mathrm{P}v}}{\omega_0 k_{\mathrm{I}v}}\dot{\phi}_{dq}+\phi_{dq}+\frac{1}{k_{\mathrm{I}v}}i_{\mathrm{g}dq}\\ &\quad-\frac{\omega}{\omega_0 k_{\mathrm{I}v}}c\mathrm{T}(\tfrac{\pi}{2})e_{dq}-\frac{1}{k_{\mathrm{I}v}}i_{\mathrm{i}dq}.\end{aligned} \tag{10d}$$

D. Network interface for GFM models

Consider the GFM inverter connected to bus i of the electrical network through a transmission line. The dynamics of the grid-side current, i.e., the current flowing from the GFM inverter's capacitor terminals to the electrical network, are described by

$$\begin{aligned}\frac{l_{\mathrm{g},i}}{\omega_0 r_{\mathrm{g},i}}\dot{i}_{\mathrm{g}dq,i} &= \Big(\frac{\omega l_{\mathrm{g},i}}{\omega_0 r_{\mathrm{g},i}}\mathrm{T}(\tfrac{\pi}{2})-\mathbb{I}\Big)i_{\mathrm{g}dq,i}\\ &\quad+\frac{1}{r_{\mathrm{g},i}}(e_{dq,i}-v_{\mathrm{g}dq,i}),\end{aligned} \tag{11}$$

and the corresponding active- and reactive-power injections at the capacitor terminals are given by:

$$p_i = e_{dq,i}^\top i_{\mathrm{g}dq,i},\quad q_i = e_{dq,i}^\top \mathrm{T}(-\tfrac{\pi}{2})i_{\mathrm{g}dq,i}. \tag{12}$$

Let $s_{\mathrm{r},i}$, $s_{\mathrm{r},0}$ denote the rated three-phase powers of the GFM inverter and the electrical network, respectively, and define:

$$\sigma_i = \frac{s_{\mathrm{r},0}}{s_{\mathrm{r},i}}. \tag{13}$$

With the above definitions, the current injection and terminal voltage at bus i of the electrical network are given by

$$i_{DQ,i} = \frac{1}{\sigma_i}\mathrm{T}(-\delta_i)i_{\mathrm{g}dq,i},\qquad v_{DQ,i} = \mathrm{T}(-\delta_i)v_{\mathrm{g}dq,i}. \tag{14}$$

V. Model-order Reduction: Deriving the Kuramoto Model

In this section, we first establish the assumptions under which the Kuramoto model can be recovered from full-order models of GFM inverters and the interconnecting electrical network. We also describe how Kron reduction is leveraged to develop a reduced-order model of the grid-side current and electrical network dynamics. With these, we present the main results of this paper, wherein singular perturbation analysis and a design choice of $\psi=\varphi$ return the Kuramoto model from the full-order model of GFM inverters and the network.

In what follows, for an interconnected collection of n GFM inverters, we adopt the notation below for GFM inverter-related signals and parameters:

$$\begin{aligned}&\delta=[\delta_1,\ldots,\delta_n]^\top, && \omega=[\omega_1,\ldots,\omega_n]^\top,\\ &K_{\mathrm{f}}=\mathrm{diag}\big(\kappa_{\mathrm{f},1},\ldots,\kappa_{\mathrm{f},n}\big), && \Sigma=\mathrm{diag}\big(\sigma_1,\ldots,\sigma_n\big),\\ &p^\star=[p_1^\star,\ldots,p_n^\star]^\top, && q^\star=[q_1^\star,\ldots,q_n^\star]^\top.\end{aligned}$$

A. Parametric assumptions

For each GFM inverter connected to a bus in the electrical network, we represent its dynamics using the universal primary control model in (9), and we make the following reasonable assumption, which is based on parameter values reported in the literature [4], [10], [13]–[15].

Assumption 1. *There exists a small parameter ϵ, as well as constants $\lambda_1,\ldots,\lambda_{14}\in(0,1]$, such that:* $\tau_{\mathrm{f}}=\lambda_1\epsilon$, $\tau_{\mathrm{v}}=\lambda_2\epsilon$, $\tau_{\mathrm{p}}=\lambda_3\epsilon$, $\kappa_{\mathrm{d}}=\lambda_4\epsilon$, $\kappa_{\mathrm{v}}=\lambda_5\epsilon$, $\frac{k_{\mathrm{P}}}{\omega_0 k_{\mathrm{I}}}=\lambda_6\epsilon$, $\frac{1}{\omega_0^2 k_{\mathrm{I}}}=\lambda_7\epsilon$, $\frac{l_{\mathrm{i}}}{\omega_0 r_{\mathrm{i}}}=\lambda_8\epsilon$, $\frac{c}{\omega_0}=\lambda_9\epsilon$, $\frac{l_{\mathrm{g}}}{\omega_0 r_{\mathrm{g}}}=\lambda_{10}\epsilon$, $\frac{k_{\mathrm{P}i}}{\omega_0 k_{\mathrm{I}i}}=\lambda_{11}\epsilon$, $\frac{k_{\mathrm{P}v}}{\omega_0 k_{\mathrm{I}v}}=\lambda_{12}\epsilon$, $\frac{1}{\omega_0 k_{\mathrm{I}v}}=\lambda_{13}\epsilon$, $\tau_\ell=\lambda_{14}\epsilon$.

Additionally, we require the following assumptions on the angular frequency of the GFM inverter, and the inductance and resistance of its filter and interconnecting lines.

Assumption 2. *The angular frequency of the GFM inverters satisfy the constraint*

$$\left|\frac{\omega_i-\omega_0}{\omega_0}\right|\leq\epsilon,\qquad\forall i=\{1,2,\dots,n\}.$$

Assumption 3. *The time constants associated with the grid-side currents of the LCL filter are equal to those associated with the transmission line currents. In otherwords, the grid-side inductive component of the LCL filter and transmission line impedances are such that:*

$$\frac{l_{\mathrm{g},i}}{r_{\mathrm{g},i}}=\tau_\ell\omega_0,\qquad\forall i=\{1,2,\dots,n\}.$$

B. Time-domain Kron-reduction

Consider an electrical network with b buses and l transmission lines, whose dynamics are described by (5). Suppose that buses 1 to n, where $n\leq b$, have a GFM inverter, whose dynamics are described by (9) and (10), connected to them, whereas buses $n+1$ to b have no additional elements connected to them. Then, without loss of generality, let the first n rows of M be associated with buses 1 to n, and the other rows be associated with buses $n+1$ to b. Accordingly, $M\in\mathbb{R}^{b\times l}$, $I_{DQ}\in\mathbb{R}^{2\times b}$, and $V_{DQ}\in\mathbb{R}^{2\times b}$ can be partitioned as follows: $M=\left[M_1^\top,\,M_0^\top\right]^\top$, $I_{DQ}=\left[I_{1DQ},\,0\right]$, $V_{DQ}=\left[V_{1DQ},\,V_{0DQ}\right]$, where $M_1\in\mathbb{R}^{n\times l}$, $M_0\in\mathbb{R}^{(b-n)\times l}$, $I_{1DQ}\in\mathbb{R}^{2\times n}$, $V_{1DQ}\in\mathbb{R}^{2\times n}$, and $V_{0DQ}\in\mathbb{R}^{2\times(b-n)}$. We define:

$$\begin{aligned}R_{\mathrm{g}}&=\mathrm{diag}\left(r_{\mathrm{g},1},\,\dots\,,\,r_{\mathrm{g},n}\right)\in\mathbb{R}^{n\times n},\\E_{DQ}&=\left[\mathrm{T}(-\delta_1)e_{dq,1},\,\dots\,,\,\mathrm{T}(-\delta_n)e_{dq,n}\right]\in\mathbb{R}^{2\times n}.\end{aligned}$$

Then, using (11), (14), and Assumption 3, the dynamics of the grid-side current of all LCL filters are described by

$$\tau_\ell\dot{I}_{1DQ}=\left(\tau_\ell\omega_0\mathrm{T}(\tfrac{\pi}{2})-\mathbb{I}\right)I_{1DQ}+(E_{DQ}-V_{1DQ})(\Sigma R_{\mathrm{g}})^{-1}.\tag{15}$$

Substituting this expression appropriately into (5), while recognizing that $I_{DQ}=\left[I_{1DQ},\,0\right]$, it follows that we obtain the following algebraic relationships:

$$\begin{aligned}0=&(V_{1DQ}-E_{DQ})(\Sigma R_{\mathrm{g}})^{-1}+V_{1DQ}M_1R^{-1}M_1^\top\\&+V_{0DQ}M_0R^{-1}M_1^\top,&\text{(16a)}\\0=&V_{1DQ}M_1R^{-1}M_0^\top+V_{0DQ}M_0R^{-1}M_0^\top.&\text{(16b)}\end{aligned}$$

The matrix $M_0R^{-1}M_0^\top$ is strictly diagonally dominant, and is therefore invertible (see e.g., [16, Corollary 5.6.17]). Following from [17, Lemma 2.1], there exists a directed graph $\mathcal{G}_{\mathrm{e}}=\left(\mathcal{V}_{\mathrm{e}},\mathcal{E}_{\mathrm{e}}\right)$ with incidence matrix $M_{\mathrm{e}}\in\mathbb{R}^{n\times|\mathcal{E}_{\mathrm{e}}|}$ and diagonal matrix $R_{\mathrm{e}}\in\mathbb{R}^{|\mathcal{E}_{\mathrm{e}}|\times|\mathcal{E}_{\mathrm{e}}|}$ such that

$$\begin{aligned}M_{\mathrm{e}}R_{\mathrm{e}}^{-1}M_{\mathrm{e}}^\top=&M_1R^{-1}M_1^\top\\&-M_1R^{-1}M_0^\top\left(M_0R^{-1}M_0^\top\right)^{-1}M_0R^{-1}M_1^\top.\end{aligned}\tag{17}$$

Consequently, if (16b) is used to solve for V_{0DQ} as a function of V_{1DQ}, the result is substituted into (16a), and (17) is used to simplify the result, we have that the electrical network dynamics are described by

$$E_{DQ}(\Sigma R_{\mathrm{g}})^{-1}=V_{1DQ}\left(M_{\mathrm{e}}R_{\mathrm{e}}^{-1}M_{\mathrm{e}}^\top+(\Sigma R_{\mathrm{g}})^{-1}\right).\tag{18}$$

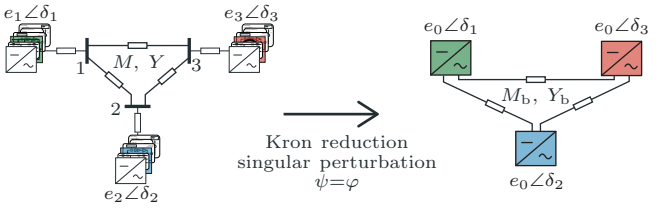

(a) Full−order model (b) Kuramoto−type model

Fig. 2: Recovering a Kuramoto-type model from the full-order model of a 3-bus GFM inverter-based power network. Connected to buses 1, 2, and 3 are a dVOC-, droop-, and VSM-based GFM inverter, respectively. Time-domain Kron reduction facilitates the systematic elimination of buses $1,2,3$, singular perturbation reduces the model order of the GFM inverter and network dynamics; and the choice $\psi=\varphi$ recovers the Kuramoto model.

The matrix $(M_{\mathrm{e}}R_{\mathrm{e}}^{-1}M_{\mathrm{e}}^\top+(\Sigma R_{\mathrm{g}})^{-1})$ is also strictly diagonally dominant, and is therefore invertible. Also, following from [17, Lemma 2.1], there exists a directed graph $\mathcal{G}_{\mathrm{b}}=\left(\mathcal{V}_{\mathrm{b}},\mathcal{E}_{\mathrm{b}}\right)$ with incidence matrix $M_{\mathrm{b}}\in\mathbb{R}^{n\times|\mathcal{E}_{\mathrm{b}}|}$ and diagonal matrix $R_{\mathrm{b}}\in\mathbb{R}^{|\mathcal{E}_{\mathrm{b}}|\times|\mathcal{E}_{\mathrm{b}}|}$ such that

$$\begin{aligned}M_{\mathrm{b}}R_{\mathrm{b}}^{-1}M_{\mathrm{b}}^\top=&(\Sigma R_{\mathrm{g}})^{-1}-(\Sigma R_{\mathrm{g}})^{-1}\big(M_{\mathrm{e}}R_{\mathrm{e}}^{-1}M_{\mathrm{e}}^\top\\&+(\Sigma R_{\mathrm{g}})^{-1}\big)^{-1}(\Sigma R_{\mathrm{g}})^{-1}.\end{aligned}\tag{19}$$

Consequently, if (18) is used to solve for V_{1DQ} as a function of E_{DQ}, the result is substituted into (15), and (19) is used to simplify the result, we have that the dynamics of the grid-side current and the electrical network are described by

$$\tau_\ell\dot{I}_{1DQ}=\left(\tau_\ell\omega_0\mathrm{T}(\tfrac{\pi}{2})-\mathbb{I}\right)I_{1DQ}+E_{DQ}M_{\mathrm{b}}R_{\mathrm{b}}^{-1}M_{\mathrm{b}}^\top.\tag{20}$$

In effect, buses with no inverters are eliminated, the bus that the GFM inverters are connected to are also eliminated, and the end result is a reduced-order network in which the capacitive elements of the LCL filters in the GFM inverters are directly interconnected. See Fig. 2 for an illustration.

C. Recovering the Kuramoto model and inferences

Consider n GFM inverters that are interconnected via an electrical network with b buses and l transmission lines. The theorem below, whose proof is excluded due to page limitations, establishes the equivalence of the GFM inverter dynamics and those of the Kuramoto model.

Theorem (The Kuramoto Model)**.** *Under Assumptions 1–3, and with a design choice of $\psi=\varphi$, the dynamics of the GFM inverters and interconnecting transmission lines can be described by the Kuramoto model*

$$\dot{\delta}=K_{\mathrm{f}}\left(p^\star\sin\varphi-q^\star\cos\varphi-e_0^2\Sigma M_{\mathrm{b}}Y_{\mathrm{b}}\mathbf{sin}\left(M_{\mathrm{b}}^\top\delta\right)\right),\tag{21}$$

where $Y_{\mathrm{b}}=\frac{1}{\sqrt{1+\tau_\ell^2\omega_0^2}}R_{\mathrm{b}}^{-1}$ is a diagonal matrix whose diagonal elements comprise magnitudes of transmission-line admittances for the Kron-reduced network, and e_0 is a scalar variable.

Note that (21) has the same structure as the Kuramoto model introduced in (1). To see the precise equivalence, let $\mathbb{L}_{\mathrm{b}}$ denote a one-to-one mapping from $\mathcal{E}_{\mathrm{b}}$ to $\mathcal{L}_{\mathrm{b}}=\{1,2,\dots,|\mathcal{E}_{\mathrm{b}}|\}$ so that, for each $(i,j)\in\mathcal{E}_{\mathrm{b}}$, there exists a unique $k\in\mathcal{L}_{\mathrm{b}}$ that satisfies $k=\mathbb{L}_{\mathrm{b}}(i,j)$. Also, let $r_{\mathrm{b},k}$

denote the k-th diagonal element of R_{b}. Then, the following terms are equivalent in both models:

$$\kappa_{\mathrm{f},i}(p_i^\star \sin\varphi - q_i^\star \cos\varphi) \equiv \omega_i - \omega_0,$$
$$\frac{e_0^2 \kappa_{\mathrm{f},i}\sigma_i}{r_{\mathrm{b},k}\sqrt{1+\tau_\ell^2\omega_0^2}} \equiv a_{ij}.$$

D. Simulation results

The three-bus networks depicted in Fig 2 are simulated using the models presented in Sections III, IV, and V. The phase and frequency response of both models are visualized in Fig. 3. With step-changes applied to the active and reactive power setpoints, the same simulation is run using the full-order model and the Kuramoto model, and responses of both models are compared. At $t = 0$ s, we have $p^\star = [-2,\ 1,\ 1]$ and $q^\star = [0.1,\ 0.4,\ -0.5]$, at $t = 2.5$ s, we have $p^\star = [-3,\ 0.5,\ 0.5]$ and $q^\star = [-0.3,\ -0.1,\ -0.1]$, and at $t = 7.5$ s, we have $p^\star = [-2,\ 1.5,\ 1.2]$ and $q^\star = [0.1,\ 0.2,\ 0.2]$. The numerical results presented in Fig 3 demonstrate that phase and frequency response of the Kuramoto-type model approximately tracks those of the full-order model.

VI. Concluding Remarks

This work demonstrated how a Kuramoto model can be recovered from the full-order model of inverter-based power networks. Specifically, three grid-forming inverter technologies were considered, namely droop control, virtual synchronous machine control, and dispatchable virtual oscillator control. Full-order models were developed for electric power networks based on them, and singular perturbation analysis as well as Kron reduction were used to derive the Kuramoto model. Simulation results indicate that the response of the Kuramoto model closely tracks that of the full-order model.

References

[1] Y. Kuramoto, "Self-entrainment of a population of coupled non-linear oscillators," in *Proceedings of the International Symposium on Mathematical Problems in Theoretical Physics*, H. Araki, Ed. Berlin, Heidelberg: Springer Berlin Heidelberg, 1975, pp. 420–422.

[2] M. C. Chandorkar, D. M. Divan, and R. Adapa, "Control of parallel connected inverters in standalone AC supply systems," *IEEE Trans. Ind. Appl.*, vol. 29, no. 1, pp. 136–143, Jan. 1993.

[3] S. D'Arco, J. Suul, and O. Fosso, "A virtual synchronous machine implementation for distributed control of power converters in smartgrids," *Electric Power Systems Research*, vol. 122, pp. 180 – 197, 2015.

[4] M. Lu, S. Dutta, V. Purba, S. Dhople, and B. Johnson, "A grid-compatible virtual oscillator controller: Analysis and design," in *IEEE Energy Conversion Congress and Exposition*, 2019, pp. 2643–2649.

[5] M. Sinha, F. Dörfler, B. B. Johnson, and S. V. Dhople, "Uncovering Droop Control Laws Embedded Within the Nonlinear Dynamics of Van der Pol Oscillators," *IEEE Trans. Control of Network Systems*, vol. 4, no. 2, pp. 347–358, Jun. 2017.

[6] A. Tayyebi, D. Groß, A. Anta, F. Kupzog, and F. Dörfler, "Frequency stability of synchronous machines and grid-forming power converters," *IEEE Journal of Emerging and Selected Topics in Power Electronics*, vol. 8, no. 2, pp. 1004–1018, 2020.

[7] P. Varaiya, F. F. Wu, and Rong-Liang Chen, "Direct methods for transient stability analysis of power systems: Recent results," *Proceedings of the IEEE*, vol. 73, no. 12, pp. 1703–1715, 1985.

[8] F. Dörfler and F. Bullo, "Synchronization and transient stability in power networks and nonuniform Kuramoto oscillators," *SIAM Journal on Control and Optimization*, vol. 50, no. 3, pp. 1616–1642, 2012.

[9] J. W. Simpson-Porco, F. Dörfler, and F. Bullo, "Droop-Controlled Inverters are Kuramoto Oscillators," *IFAC Proceedings Volumes*, vol. 45, no. 26, pp. 264–269, 2012, 3rd IFAC Workshop on Distributed Estimation and Control in Networked Systems.

[10] O. Ajala, A. Domínguez-García, and P. Sauer, *A Hierarchy of Models for Inverter-Based Microgrids*. Springer-Verlag, Berlin, 2017.

[11] P. Kundur, N. J. Balu, and M. G. Lauby, *Power System Stability and Control*. McGraw-Hill, 1994.

[12] A. Yazdani and R. Iravani, *Voltage-Sourced Converters in Power Systems*. Wiley, Jan. 2010.

[13] L. Luo and S. V. Dhople, "Spatiotemporal model reduction of inverter-based islanded microgrids," *IEEE Trans. Energy Convers.*, vol. 29, no. 4, pp. 823–832, Dec. 2014.

[14] P. Vorobev, P. Huang, M. A. Hosani, J. Kirtley, and K. Turitsyn, "High-fidelity model order reduction for microgrids stability assessment," *IEEE Trans. Power Syst.*, vol. 33, no. 1, pp. 874–887, Jan 2018.

[15] I. Caduff, U. Markovic, C. Roberts, G. Hug, and E. Vrettos, "Reduced-order modeling of inverter-based generation using hybrid singular perturbation," *Electric Power Systems Research*, vol. 190, p. 106773, 2021.

[16] R. A. Horn and C. R. Johnson, *Norms for vectors and matrices*. Cambridge University Press, 1985, p. 257–342.

[17] S. Y. Caliskan and P. Tabuada, "Kron reduction of power networks with lossy and dynamic transmission lines," in *Proc. of the IEEE Conference on Decision and Control (CDC)*, 2012, pp. 5554–5559.

TABLE II: Model Parameter Values.

e_0	l_{i}	l_{g}	c	r_{i}	r_{g}	$k_{\mathrm{P}v}$	$k_{\mathrm{I}v}$	$k_{\mathrm{P}i}$	$k_{\mathrm{I}i}$	κ_1	κ_2	d_{f}	d_{v}	d_{d}	m_{f}	ω_{c}	k_{P}	k_{I}
1	0.02	0.02	0.11	0.014	0.014	1.45	10.29	0.98	0.69	0.003	0.046	0.8	25	0.005	0.01	125.7	50	1

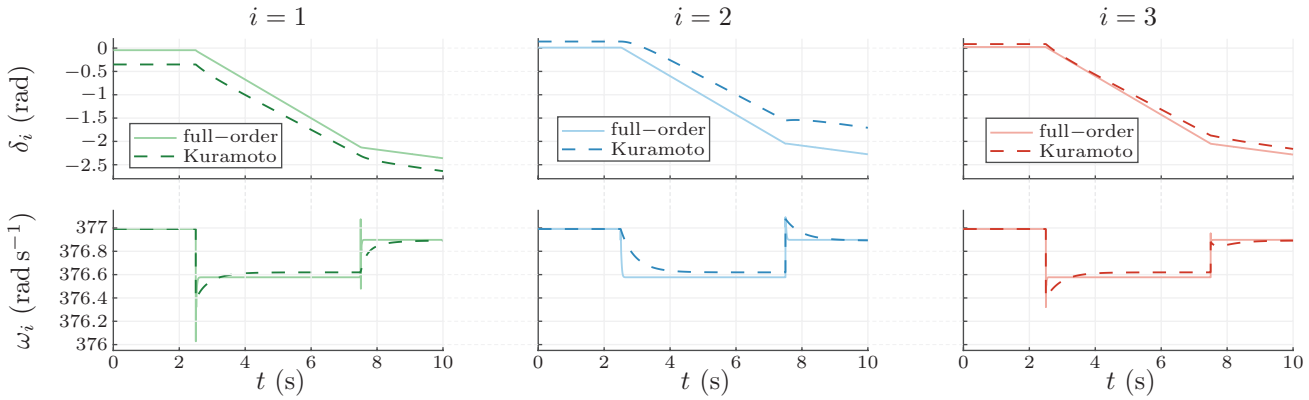

Fig. 3: Phase and frequency response of the full-order and Kuramoto models depicted in Fig. 2. The full-order GFM models are adopted from Fig. 1.